JOURNAL OF MATERIALS SCIENCE 10 (1973) 1904–1919

Fracture toughness and thermal shock of tool and turbine ceramics

Y. W. MAI, A. G. ATKINS*
Department of Mechanical Engineering, University of Michigan, Ann Arbor, Michigan, USA

The behaviour of some commercial tool carbides and turbine ceramics has been investigated in regard to resistance to crack initiation, crack propagation and retained strength after thermal shock. New data are provided, particularly measurements of the fracture toughness of these materials at actual operating temperatures (up to 1200° C). Many of the materials did not follow the generally accepted Hasselman theory for thermal shock in ceramics, and instead of showing a discontinuity in retained strength at some critical quenching temperature difference, their residual strengths fell gradually at temperatures lower than their supposed critical quenching temperature. This behaviour is explicable when high temperature toughnesses, strengths and moduli are used in the damage resistance parameter (ER/σ_f^2). It seems that materials not following the Hasselman model suffer cumulative damage with increasing number of shocks. Sub-critical crack growth occurs even if $(K_{IC}/\sigma_f)^2$ values are constant, and such damage, which reduces the room temperature retained strength, is enhanced by $(K_{IC}/\sigma_f)^2$ decreasing at temperatures below ΔT_c. In contrast, materials obeying Hasselman's model appear to have a constant $(K_{IC}/\sigma_f)^2$ below ΔT_c and for some temperature range above. Only then are "one-shock" characterizations of materials possible, otherwise, the retained strength depends upon the number of prior shocks. Experiments are also reported which describe the effects of rate of testing on the unshocked and shocked mechanical properties of ceramics. Oxidation is shown to influence the results in a manner not obvious from single shock tests.

List of symbols

α	Linear thermal expansion coefficient
h	Heat transfer coefficient
k	Thermal conductivity
σ_f	Tensile fracture strength
σ_T	Thermal shock induced tensile stress
σ_a	Retained strength of thermally shocked testpiece
E	Young's modulus
E_0	Young's modulus of crack-free material
ν	Poisson's ratio
B	Biot modulus $= ah/k$
a	Half thickness, or radius of thermal shocked body
ΔT_c	Critical shock temperature difference
r_0, r_f	Radius of circular flaws. Subscripts 0 and f refer to initial and final conditions
N	Crack density
R^*, R	Fracture surface energies (fracture toughness)
V	Volume of material under strain
P	Load
u	Displacement
K_{IC}	Critical stress intensity factor for mode I fracture
$\dot{L}$	Crack velocity
N_f	Number of thermal cycles to failure

1. Introduction

Ceramics very often fail in service because

* Present address: Delta Materials Research Ltd, Box 22, Hedleigh Road, Ipswich, Suffolk, UK.

fractures induced by thermal shocks either break the part in one go, or degrade the retained strength cumulatively. Although many studies have been made of thermal shock fractures in refractories [1–2] and oxides of ceramics [3–5], only limited research has been published on the thermal shock behaviour of those ceramics commonly used for cutting tools and as turbine materials. The present paper concerns these latter two types of ceramic.

One traditional type of thermal shock test consists in successively plunging a small specimen a number of times from some high temperature into a cold fluid and then looking for surface cracks. The temperature from which the quenchings take place is increased and the process repeated until cracks are observed. The final temperature at which cracks are initiated is used to rank materials for given geometries and environments (i.e. quenching media). The type and size of specimen, and the heating and quenching schedules, vary from worker to worker and are arbitrary. Such tests are sometimes continued at increasing temperature intervals until the already initiated cracks propagate in shock so that the specimens break completely. Then, in addition to the merit ranking based upon crack initiation, some idea of the life of the part is available by adding up the total number of heating and quenching cycles to failure. Insofar as the heating and quenching schedules are arbitrary, the results are quite empirical.

Another type of thermal shock evaluation measures the room temperature strength that test-pieces (usually three-point bend specimens) retain after they have been shocked. Such experiments are used particularly to investigate the Hasselman theory [3, 4] of thermal shock.

A generalized theory of thermal-shock-induced failure has been developed by Hasselman, in which both aspects of crack initiation and propagation are covered [3]. A body is considered to have many mechanical flaws in the form of penny shaped Griffith microcracks of radius r_0. There are N/unit volume. The body is presumed to undergo a given thermal shock rapid temperature change with mild heat transfer conditions (i.e. the Biot modulus, $B = ah/k$, is small). The critical stress to cause crack initiation is given by:

$$\sigma_f = \frac{\pi}{2}\sqrt{\left[\frac{E_0 R}{\pi r_0(1-\nu^2)}\right]}. \quad (1)$$

By considering the potential energy of the body at crack initiation, together with the maximum thermal stress induced by a given thermal shock, it is possible to predict that a critical shock temperature difference (ΔT_c) is required to initiate all N cracks, where

$$\Delta T_c \geqslant \frac{1.625}{\alpha}\,\frac{k}{ah}\sqrt{\left[\frac{\pi R(1-\nu)}{r_0 E_0(1+\nu)}\right]}\left[1+\frac{16r_0^3(1-\nu^2)N}{3}\right]. \quad (2)$$

It is seen that ΔT_c for crack initiation is proportional to $k\sigma_f/(\alpha E)$ a fact which may be deduced also from simple considerations of thermal stresses in crack-free bodies [6, 7]. Notice that for long cracks ΔT_c also increases with N.

The events subsequent to crack initiation either may involve catastrophic propagation giving complete rupture, or may involve crack arrest after some propagation, where excess energy at initiation (converted into crack kinetic energy), is ultimately absorbed by the body so that the cracks arrest. If all N penny cracks grow from r_0 to an arrested radii r_f, it may be shown that [3]

$$r_f = \frac{1}{2\sqrt{2}}\left[\frac{R/R^*}{Nr_0(1-\nu^2)}\right]^{1/2} \quad (3)$$

for $r_f \gg r_0$, thus

$$r_f = \sqrt{\left(\frac{1}{2\pi N}\right)\cdot\left(\frac{E_0 R^*}{\sigma_f^2}\right)}^{-1/2} = \sqrt{\left[\frac{1}{2\pi N(1-\nu^2)}\right]}\left(\frac{K_{IC}}{\sigma_f}\right)^{-1} \quad (4)$$

using Equation 1. r_f indicates the damage or extent of crack propagation, so that materials in which r_f is kept small have good thermal shock damage resistance. In this way, large $(ER^*/\sigma_f^2) = (K_{IC}/\sigma_f)^2 \cdot (1-\nu^2)$† and large N promote thermal shock resistance. Notice that R^* (the average dynamic work of fracture in the shock environment) is not necessarily the same as R for initiation; in the absence of precise values, it is, however, customary to assume that $R^* = R$.

Subsequent room temperature testing of materials shocked above ΔT_c show a degraded strength as the fracture loads are those to break testpieces containing larger r_f cracks rather than

† ER^*/σ_f^2 or $(K_{IC}/\sigma_f)^2$ in fracture mechanics describes the size of the plastic zone at the crack tip [8]. Recent research shows also that the group characterizes the transition of quasi-static cracking to generalized yielding [9], and that it can rank the machinability of materials [10].

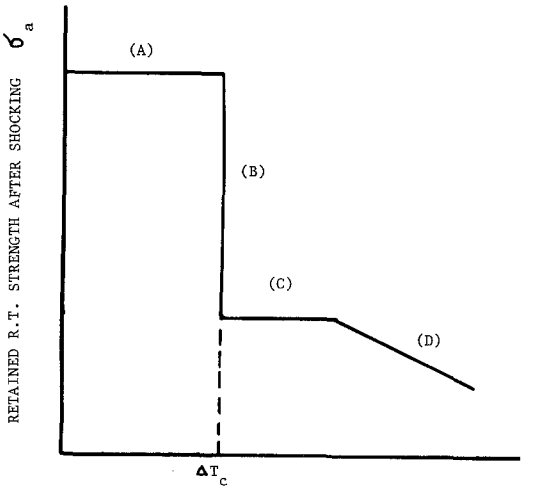

Figure 1 Schematic representation of strength behaviour versus thermal shock severity (after Hasselman [31]. (A) Constant "as-received" strength, no fracture initiation caused by shock. (B) Instantaneous decreases in strength (crack propagation and arrest). (C) Constant strength (previously arrested cracks now sub-critical for these ΔT). (D) Gradual decrease in strength as cracks get longer.

smaller r_0 cracks. Fig. 1 shows schematically the after-shock strength behaviour against the shock severity according to the Hasselman theory. It should be noted that only single shocks (as opposed to a number of repeated shocks from a given temperature) are necessary to characterize a material obeying this model since short initial flaws, once initiated by the critical temperature difference, spread quickly to larger arrested cracks which are then "sub-critical" until very much larger thermal shock temperature differences. Thus, the retained strength after shocks bigger than ΔT_c for some range is constant (region C), since the arrested r_f cracks are sub-critical for additional propagation in this range of temperature. It may be shown [11] that the fractional retained strength of a rectangular beam, after the critical shock is approximately given by:

$$\frac{\sigma_a}{\sigma_f} = \left[\frac{1.28}{\pi}\,\frac{NE^2R^2E_0R^*}{(1-\nu^2)^2\sigma_f^6}\right]^{1/4}. \qquad (5)$$

If it be assumed that $E_0 = E$ and $R^* = R$, we have

$$\sigma_a/\sigma_f \propto N^{1/4}(K_{IC}/\sigma_f)^{3/2} \qquad (6)$$

so that the strength loss $(\sigma_f - \sigma_a)/\sigma_f$ may be correlated with $(K_{IC}/\sigma_f)^2$.

Experiments in support of the model may be found in Hasselman [4], Davidge and Tappin [12] and Gupta [5] for single crystal sapphire and for polycrystalline Al_2O_3 of various grain sizes; in Gupta [13] for a hot-pressed ZnO; and in Coppola *et al.* [14] for aluminosilicate and soda-lime glass. It should be noted that magnitudes of the controlling parameters, such as ER^*/σ_f^2 or $(K_{IC}/\sigma_f)^2$ etc, in these studies have been worked out using *room temperature* values of the modulus, toughness and strength. High temperature values are often not known, but as will be demonstrated later in this paper, variations in E, R or σ_f with temperature, affect the response of materials to shock, and lead to marked deviations from the Hasselman model.

Not all ceramics precisely follow the Hasselman model. For example, Ainsworth and Herron [2] have shown that after-shock strength loss of steel-works refractories depends on the number of shocks, the retained strength levelling off only after some 10 to 15 cycles; the model suggests that one shock from the critical level should do all the damage. In the experiments reported in this paper, we find that repeated shocks at a constant quenching temperature difference cause cumulative strength degradation, when compared with a single shock. The strength retained after shock is proportional to the one-fourth power of crack density (Equation 6). Experiments show that the crack density usually increases with the quenching temperature difference and the number of shocks (see for example the study [15] on polycrystalline Al_2O_3). At more severe shocks, some cracks will coalesce during spreading thus reducing the crack density and increasing the average crack length. The combined result must be to produce reductions in predicted strength.

The present work also shows that not all ceramics show an instantaneous strength degradation at a critical ΔT_c. Some materials show a gradual reduction in retained strength at increasing shock temperature differences. Explanations for this behaviour may be given, however, if due account is taken of temperature (and possible rate) variations in modulus, strength and fracture toughness. Oxidation also influences retained strength as will be shown.

This paper, therefore, presents new data not only on the thermal shock behaviour of some tool and turbine ceramics, but also on other mechanical property variations with temperarure and rate – particularly fracture toughness. Sensible overall interpretations follow by using such data in the thermal shock analysis.

2. Experiments

2.1. Materials

The ceramics studied may be divided into two groups, namely those used in turbine applications (M19, magnesium–aluminium–silicate, $2MgO2Al_2O_35S_iO_2$; Owens Illinois "Cer Vit" (Registered Name) C140 and C132, lithium–aluminium–silicates), and those used in cutting (Nippon A2, a hot-pressed alumina mixed with titanium carbide, 70 Al_2O_3 30 TiC percent; Adamas Co. Titan 60 and Titan 80, both titanium carbides with Ni–Mo binder; Kennametal K96, a tungsten carbide with cobalt binder; and two lots of GE Carboloy 370, a tungsten carbide blended with cobalt, WC/TiC/TaC/Co, 72/8/11.3/8.5% by weight, one dense commercial tool material, the other a specially made up lower density material).

For various reasons, the materials were used in various sizes and shapes, some specially prepared, some directly in the as-bought commercial tool insert size and shape. Because of the difficulty of obtaining large pieces of these solids, much thought was given to the best use of the available samples, and suggestions are given later regarding fracture toughness testpieces.

2.2. Thermal shock tests

Specimens with dimensions 12.7 mm × 12.7 mm × 4.7 mm were subjected to repeated cycles of heating and quenching until fracture occurred. Heating was performed in an electric furnace (about 20 to 30 min being allowed to reach equilibrium) and quenching in a water bath at about 20° C. Each specimen was first subjected to 10 thermal cycles with a furnace temperature of 800° C. If it survived this treatment, 10 cycles were repeated in succession from furnace temperatures at 900, 1000, 1100 and 1200° C, until failure occurred. Surface cracks were observed in a × 20 optical microscope.

2.3. High temperature strength measurements

Three-point bend specimens of dimensions 31.8 mm × 2.54 mm × 2.5 mm (25.4 mm span) and 12.7 mm × 2.54 mm × 2.54 mm (10 mm span) for the turbine and cutting tool ceramics respectively were spark eroded from small commercial rectangular blocks. Testpieces were broken in an Instron testing machine at a cross-head speed of $8.33\,\mu m\,sec^{-1}$ and values of the tensile fracture strength (σ_f) were obtained at temperatures ranging from 400 to 1100° C.

2.4. Room temperature after shock strength measurements

Three-point specimens similar to those just described were shocked for 10 cycles at temperatures within the range of 400 to 1200° C (at 100° C intervals). The shocked specimens were then dried and broken at room temperature in three-point bending, at a cross-head speed of $8.33\,\mu m\,sec^{-1}$. Some experiments were also performed to investigate the effects of strain rate and number of repeated shocks on the residual strength of the shocked ceramics.

2.5. Fracture toughness measurements

Ceramic testpieces are usually small, so that because of the materials' relatively low resistance to crack propagation, cracking is often fast and catastrophic. Were it possible to control crack propagation in ceramics (which would be feasible in large correctly designed testpieces), incremental values for the work of fracture per unit area of crack growth (i.e. R) could be measured, and possible variations in R with crack velocity established [16]. Valid toughnesses obtained in this way must be measured when the cracking is stable, otherwise upper-bounds on R are obtained [17]. Thus, taking the stored strain energy at fracture of a ceramic specimen (i.e. the triangular load area under a deflection diagram) that breaks catastrophically is probably an upper bound on some average R. The shape of the testpiece is important in questions of crack stability, every specimen having its own "geometric stability factor" (g.s.f.) [16, 18, 19]. Rate dependence in R also affects stability, (i.e. the sign of $dR/d\dot{L}$ where $\dot{L}$ is crack velocity), as does the stiffness of the testing machine [18]. It may be shown that even with quite stiff machines, the smallness of most available ceramic specimens causes difficulties in promoting stable cracks, in which case upper-bound "triangular areas" are the best one can hope for [17]. Nevertheless, fracture mechanics formulae for stress intensity factors (K) of given testpiece geometries with starter cracks can be employed to determine toughness, $K_{IC}^2 = ER/(1-\nu^2)$, even if the test is catastrophic. We may note in passing that the Griffith formula (strictly applicable only to small through-cracks in a large plate stressed at its boundaries) is an inherently unstable situation; other crack geometries need not be [18].

Adaptions of commercially available ceramic shapes that should tend to be stable are shown in

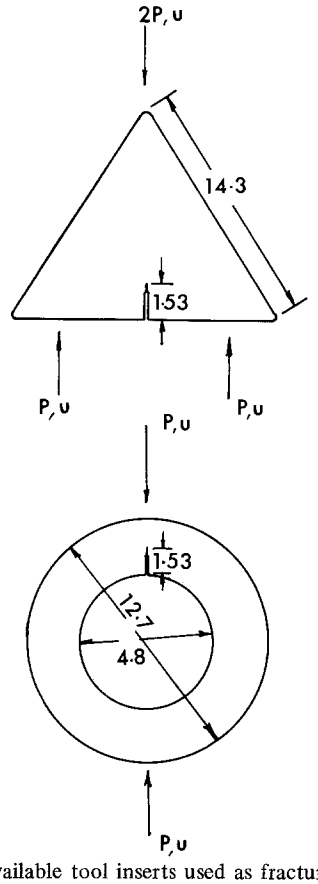

Figure 2 Available tool inserts used as fracture toughness testpieces (all dimensions in mm, 4.8 mm thick).

Fig. 2, where the starter slots were spark machined. When stable cracking occurred, R values were picked up by Gurney's irreversible work area method (Fig. 3a) [16–19]. If unstable cracking occurred, (either because of badly prepared crack fronts, negative $dR/d\dot{L}$, or because of the relatively large amount of strain energy stored in the testing machine compared with that in the (small volume) ceramic testpiece), R values could be obtained by using different starter crack lengths and constructing the presumed (unstable) constant R locus (Fig. 3b). Unfortunately, except for the slotted three-point bending test, no stress intensity factors are readily available for the two geometries in Fig. 2. In the case of Kennametal K96, values of K_{IC} were obtained using the appropriate Gross-Srawley expression for the three-point bend critical stress intensity factor [20]. Much later in our investigation, we discovered that small "part-through" elliptical starter cracks could be successfully introduced into our carbide ceramics using a Vickers hardness indenter, as suggested by Ingelstrom and Nordberg [21] and Kenny [22]. This enabled us to determine K_{IC} (and hence initiation R values) for some of our ceramics. Additionally, it was possible to investigate the fracture surfaces of those bend specimens (without starter cracks) that were used for determination of σ_f and σ_a and establish the size of the flaw from which the final break initiated. Use of "part-through" crack K_{IC} formulae for bend bars enabled extra estimates of the toughness at temperature to be gained.

Our toughness determinations thus come from a variety of sources, but all were found to be reasonably self consistent. Note that traditional methods of fracture toughness determination for ceramics are given in references [23–28].

3. Results and discussion

3.1. Traditional thermal shock evaluations

Table I summarizes the results of the thermal shock tests. The details of shock resistances for the turbine and cutting tool ceramics are given in [17]. From these experiments, it is possible to rate the ceramics according to both their resistance to crack initiation and their resistance to crack

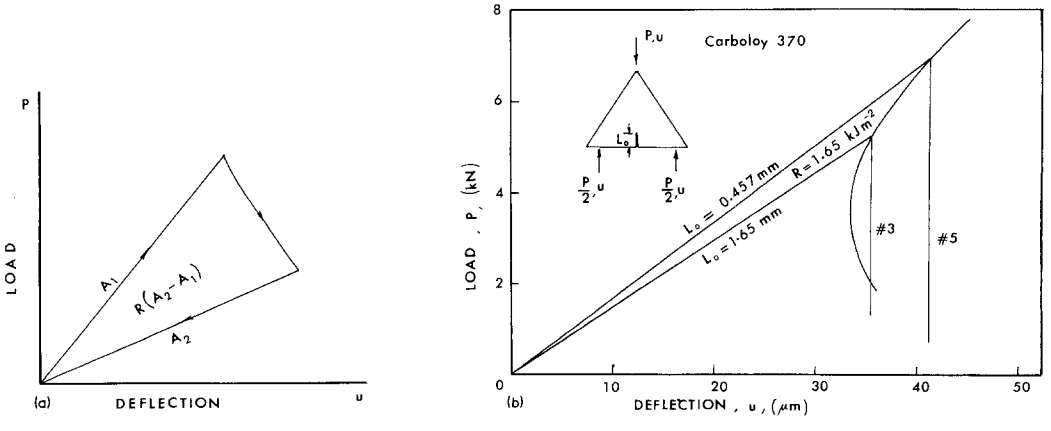

Figure 3 (a) and (b) Fracture toughness determination using Gurney's irreversible work area method.

TABLE I Evaluation of thermal shock resistances

Material	Physical properties (R.T.)				Thermal cycles completed before failure				
	α $10^{-6}\,^{\circ}C^{-1}$	k (cal m^{-1} sec^{-1} $^{\circ}C^{-1}$)	E (GN m^{-2})	σ_f (MN m^{-2})	800° C	900° C	1000° C	1100° C	1200° C
M19	2.84	0.447	20.7	32	10	10	10	10	10*
C140	−0.27	0.65	74.5	193	10	10	10	10	10*
C132	−0.27	0.65	71.9	207	10	10	10	10	1
Carboloy 370	6.57	11.00	560	1930	10†(10)	10	4		
Titan 80	7.80	5.10	428	1240	10†(3)	7			
Titan 60	7.80	5.10	428	1450	10†(3)	10			
Nippon A2	7.80	4.10	310	800	10†(2)	4			

* No failure recorded.
† Number in parentheses indicates cycles for initiation of surface cracks.

TABLE II Shock quantifying parameters of ceramics

Material	Bend strength (GN m^{-2})	$k\sigma_f/E\alpha$ (cal m^{-1} sec^{-1}) × 10^{-2}	R.T.$(K_{IC}/\sigma_f)^2$ (mm)	N_f (cycles)
M19	0.032	1.29	1.628	> 50
Nippon A2	0.800	13.20	0.378	14
Titan 80	1.240	19.00	0.041	17
Titan 60	1.450	22.20	0.097	20
C132	0.207	62.00	0.736	43
C140	0.193	56.00	0.865	> 50
Carboloy 370	1.930	66.50	0.381	24
Kennametal K96	1.720	119.00	0.374	

propagation (i.e. extent of damage). For crack initiation caused by thermal shock, the appropriate parameter is $k\sigma_f/E\alpha$, listed in the third column of Table II. The larger this number, the lesser chance that flaws will be initiated. For the tool ceramics (which have small Biot moduli) the order of decreasing merit is Carboloy 370, Titan 60, Titan 80 and Nippon A2. These predictions are in agreement with results shown in Table I for data concerning the onset of crack initiation. In the case of turbine ceramics (with rapid heat transfer conditions) M19, C140 and C132 are good thermal shock resistant materials. Although M19 has the smallest $k\sigma_f/E\alpha$, it yet possesses a high resistance to crack initiation and propagation. In light of its porous structure, these results are not unexpected.

As given in Table II, the crack initiation resistance of the cutting ceramics increases with bend strength (σ_f). For design against crack nucleation, Carboloy 370 would be chosen as the best cutting tool material.

Damage resistance or extent of crack propagation by thermal shocks is characterized by (ER^*/σ_f^2) or $(K_{IC}/\sigma_f)^2$, listed in the 4th column of Table II. The greater this number, the better is its resistance to crack propagation. The number of cycles to complete failure of the ceramics taken from Table I is shown in the 5th column. It may be seen that in general the greater the magnitude of $(K_{IC}/\sigma_f)^2$, the greater the value of N_f. In order of decreasing merit, these are M19, C140, C132, Carboloy 370, Titan 60, Titan 80 and Nippon A2. Note that Carboloy 370 previously chosen as the best cutting tool ceramic against crack initiation is also a good material on the criterion of crack damage. Conversely, although M19 possesses good damage resistance to thermal shock its use is highly limited because of its relatively weak strength of 32 MN m^{-2}.

We observe that similar values for $(K_{IC}/\sigma_f)^2$ can be produced by materials with different absolute values of K_{IC} and σ_f (cf. A2, K96 and 370). The best materials for thermal shock damage resistance are those simultaneously possessing both high toughness and high strength. Such combinations of properties may be achieved with suitable ceramic microstructures. This warrants further investigation on the possible effects of grain size, porosity, reinforced-fibres etc. on tool materials in relation to thermal shock.

3.2. Effects of thermal shock and high temperature on the bend strength of ceramics

Retained room temperature strength versus shocking temperature interval results are shown in Fig. 4a to d respectively, for the Titan 80, Titan 60, Nippon A2 and Carboloy 370 cutting tool ceramics. The first three all follow the Hasselman model, more or less, with a critical quenching temperature interval beyond which there is a marked reduction in residual bend strength. From Table III, the critical quenching temperature differences for Titan 60 and Titan 80 are 427 and 368° C respectively. The small values of the effective crack lengths ($r_0 = 1.6$ to 1.8×10^{-4} m) as estimated from Equation 1 for both carbides explains the catastrophic spreading and arrest behaviour at ΔT_c. The experimental values of critical quenching temperature difference obtained for Titan 80 and Titan 60 as inferred in Fig. 4a and b are in very good agreement with theory. Also, the predictions of retained strength given by the Hasselman model (Equation 5) agree quite well with the experiments (Table IV). The results show that Titan 60 is better than Titan 80 as far as ΔT_c is concerned. For Nippon A2, some of the testpieces broke during shocking, when the shock temperatures were above 500° C. At a quenching temperature difference of 380° C (i.e. 400 − 20° C), the strength retained after ten thermal cycles was about 15% of the unshocked specimen tested at room temperature, which was close to that predicted by the Hasselman model. Unfortunately, our data on Nippon A2 is limited but the theoretical critical quenching temperature difference of 253° C (i.e. shock temperature of 273° C) is not unreasonable. The unshocked high temperature strength of Titan 80 remains relatively constant to temperatures beyond the critical temperature (Fig. 4a).

TABLE III Estimation of critical quenching temperature difference (ΔT_c) and effective crack length (r_0)

Material	Biot modulus ($B = ah/k$)	ΔT_c (° C)	r_0 (10^4 m)
M19	28.40	217	13.00
C132	19.50	7150	6.17
C140	19.50	6450	7.25
370	1.15	1280	1.30
A2	3.10	253	3.96
Ti60	2.50	427	1.81

Note: For $B > 5.0$, $\Delta T_c \approx \sigma_f(1-\nu)/(E\alpha)$; for $B < 5.0$, $\Delta T_c \approx [3.25(1-\nu)/(ah)]\ (k\sigma_f/E\alpha)$.

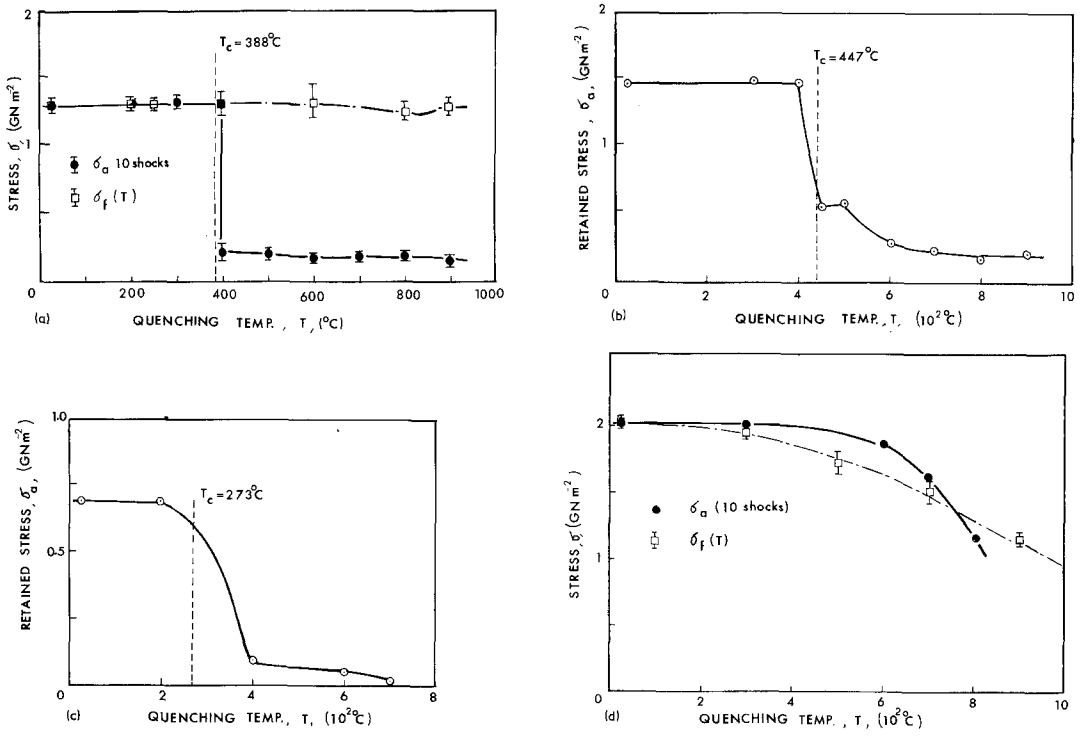

Figure 4 (a) Thermal shock and high temperature strength for Titan 80. (b) Thermal shock strength for Titan 60. (c) Thermal shock strength for Nippon A2. (d) Thermal shock and high temperature strength for the higher density Carboloy 370.

TABLE IV Predictions of strength retained after thermal shock

Material	σ_f (GN m^{-2}) (R.T.)	σ_a/σ_f		N (cracks m^{-3})
		Observed	Calculated	
Nippon A2	0.800	0.140	0.194	6×10^8
Titan 80	1.240	0.139	0.100	6×10^9
Titan 60	1.450	0.143	0.120	2.4×10^9
Carboloy 370	1.930	0.605		

The behaviour of the higher density Carboloy 370 in Fig. 4d, as reported in [11], is very interesting. The theoretical ΔT_c is some 1280° C and the effective crack length is $r_0 \approx 4 \times 10^{-2}$ cm, which for $N < 1000$ occurs to the left of the stability minima in [3], thus suggesting an instantaneous retained strength degradation only upon shocking from temperatures greater than 1300° C. However, there is a gradual reduction in residual strength for temperatures much lower than 1300° C, and in general terms it is not possible to distinguish between the bend strengths *measured* at high temperatures and those measured at room temperature after having been shocked from similar high temperatures. Above 800° C, 370 is oxidized and thermally expanded on all sides, which could very well explain the gradual strength loss above 800° C. The lower density Carboloy 370 had much lower retained strengths, particularly after repeated shocking. The results are illustrated in Fig. 10, and discussed later in Section 3.5.

Gradual after-shock strength loss behaviour (similar to the higher density Carboloy 370), which is at variance with the Hasselman model, is shown by the turbine ceramics, Fig. 5a to c. While M19 and C140 do not show any strength degradation when tested at high temperatures (700 to 1100° C) in the as-received unshocked condition, C132 does exhibit significant strength loss as the temperature increases. A plausible reason is the occurrence of subcritical crack growth and plastic flow at such flaws. This assumption is substantiated by evidence shown in some load–deflection diagrams which display obvious non-linearities before final fracture. The strength retained by the shocked specimens (i.e. after ten thermal cycles at a given quenching temperature difference) decreases gradually with increasing shock temperature for all three ceramics. Of the two cordierites,

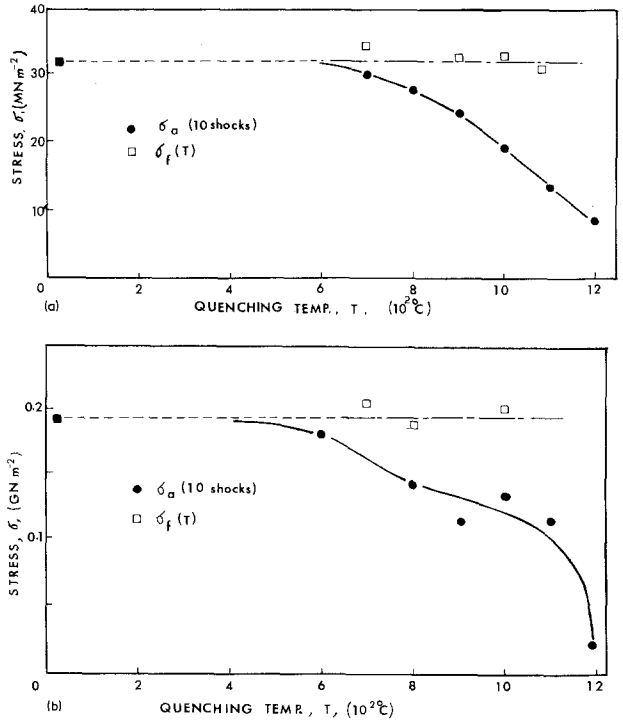

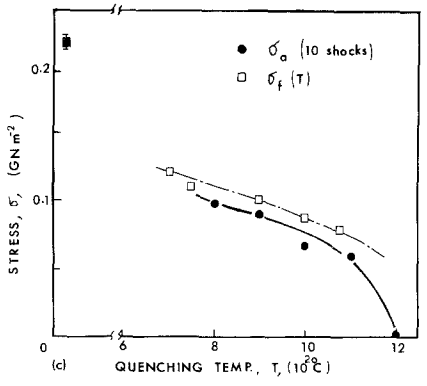

Figure 5 Thermal shock and high temperature strength for (a) M19, (b) C140 and (c) C132.

the results show that C140 should be superior at high temperatures.

In summary, the variation of retained strength after thermal shock is divided into two characteristic behaviours: (1) materials possessing a gradual strength degradation as the quenching temperature difference increases; (e.g. Carboloy 370, C140, M19); (2) materials with instantaneous strength drop at critical quenching temperature difference (e.g. Nippon A2, Titan 60 and Titan 80).

3.3. Fracture toughness results

As explained in Section 2.5, our toughness data were obtained by various techniques. A summary of the results is given in Table V. Some additional results on rate effects in K_{IC} are given in Section 3.6 later. The toughest tool carbides are Carboloy 370 and Kennametal K96, followed by Nipon A2, Titan 60, with Titan 80 the most brittle. The turbine ceramics all have low toughness, the best (C140) corresponding with the toughness of Titan 80.

Fig. 6a shows the elliptical starter crack produced by a Vickers indentation in Titan 80. The subsequent fracture surface resulted from breaking in three-point bending at 600° C. Fig. 6b and c show the flaws from which final structure in unnotched three-point bending took place at room temperature in Nippon A2 and 700° C in

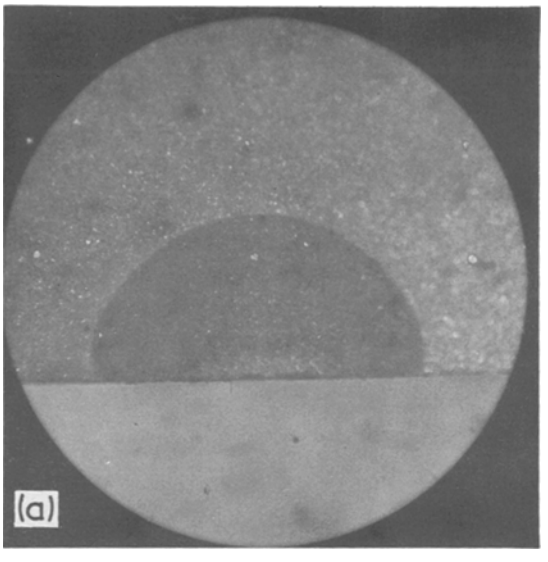

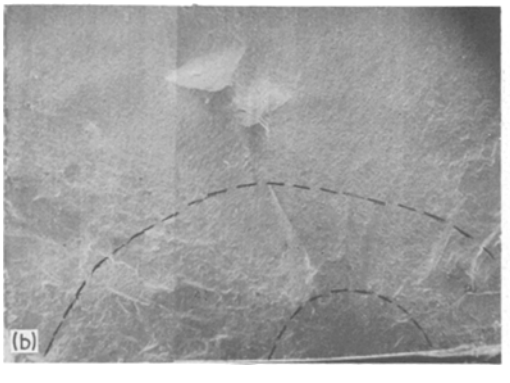

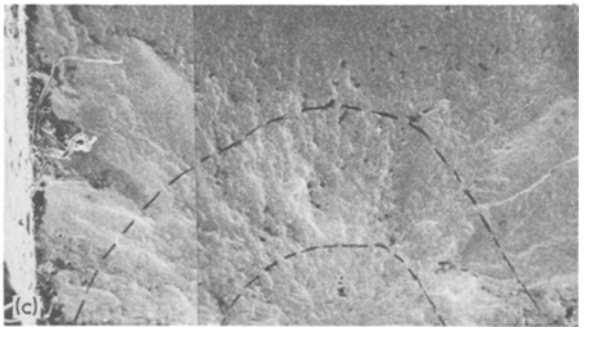

Figure 6 Typical initial flaw geometries for (a) Titan 80 (× 36); (b) Nippon A2 (× 30) and (c) Carboloy 370 (× 30).

Notes to Table V

(a) Three-point bend notched by spark erosion K_{IC} formula in [20]. R derived from $(1-\nu^2)(K_{IC}^2/E)$.

(b) Precracked by hardness indentation technique K_{IC} formulae in e.g. [21]. R derived from $(1-\nu^2)(K_{IC}^2/E)$.

(c) Three point bend unnotched high temperature test. Final flaw size determined after test. K_{IC} formulae in [20, 21]. R derived from $(1-\nu^2)(K_{IC}^2/E)$.

(d) Diametrical compression of cracked ring [16, 28], to determine R. K_{IC} derived from $\sqrt{[ER/(1-\nu^2)]}$.

(e) Bending of precracked triangular testpiece [17] to determine R. K_{IC} derived from $\sqrt{[ER/(1-\nu^2)]}$.

(f) After-shock three-point-bend test. Final flaw size determined after test. K_{IC} formulae in [20, 21]. R derived from $(1-\nu^2)(K_{IC}^2/E)$.

E values for conversions between R and K_{IC} are given in Table I. Except for C140, the room temperature E were applicable at higher temperatures. For C140 see Section 3.5.

* Number in brackets after temperature is the number of repeated shocks.

† Toughness testing performed in the presence of liquid water.

TABLE V Fracture toughness values for various ceramics

Material	Temperature (° C)	No. of Test	K_{IC} (MN m$^{-3/2}$)	R (kJ m^{-2})	Test method
Kennametal K96	22-200	6	23.33	1.030	a
Nippon A2	R.T.	3	14.65	0.820	c
	400(10)*	2	15.70	0.914	f
	600(10)	2	12.00	0.540	f
Titan 60	R.T.	3	12.80	0.455	c
	400(10)	2	13.00	0.460	f
	500(10)	2	13.70	0.518	f
	600(10)	2	11.70	0.387	f
	800(10)	2	11.40	0.365	f
Titan 80	R.T.	2	10.40	0.213	c
	400(10)	2	8.20	0.195	f
	500(10)	2	5.80	0.098	f
	600(10)	2	6.10	0.108	f
	900(10)	2	5.80	0.098	f
	R.T.	3	5.00	0.072	b
	350	3	4.50	0.059	b
	400	2	4.30	0.054	b
	600	3	5.00	0.072	b
	800	3	4.60	0.062	b
Carboloy 370	R.T.	3	27.20	1.640	e
	R.T.	2	25.60	1.430	d
	R.T.	2	28.00	1.660	b
	R.T.	2	28.50	1.715	c
	R.T.†	2	18.10	0.695	e
	400	1	11.50	0.292	b
	600	1	10.50	0.244	b
	700	2	28.50	1.715	c
	800	2	24.00	1.390	b
	900	1	28.00	1.660	b
	500(15)	2	16.90	0.607	f
	600(10)	2	22.70	1.090	f
	700(15)	2	24.00	1.220	f
	700(15)	2	18.50	0.732	f
	760(10)	2	28.10	1.675	f
M19	R.T.	3	1.12	0.074	c
	800	2	1.08	0.074	c
	900	2	1.04	0.065	c
	1000	2	0.88	0.061	c
	1100	2	0.76	0.054	c
	1200	2	0.38	0.045	c
	800	2	1.00	0.059	f
	1000	2	1.18	0.081	f
	1100	2	1.27	0.094	f
C140	R.T.	3	5.42	0.500	c
	600	2	5.35	0.500	c
	700	2	5.30	0.500	c
	800	2	4.88	0.500	c
	900	2	4.29	0.480	c
	1000	2	3.55	0.480	c
	1100	2	2.90	0.470	c
C132	R.T.	3	5.20	0.430	c

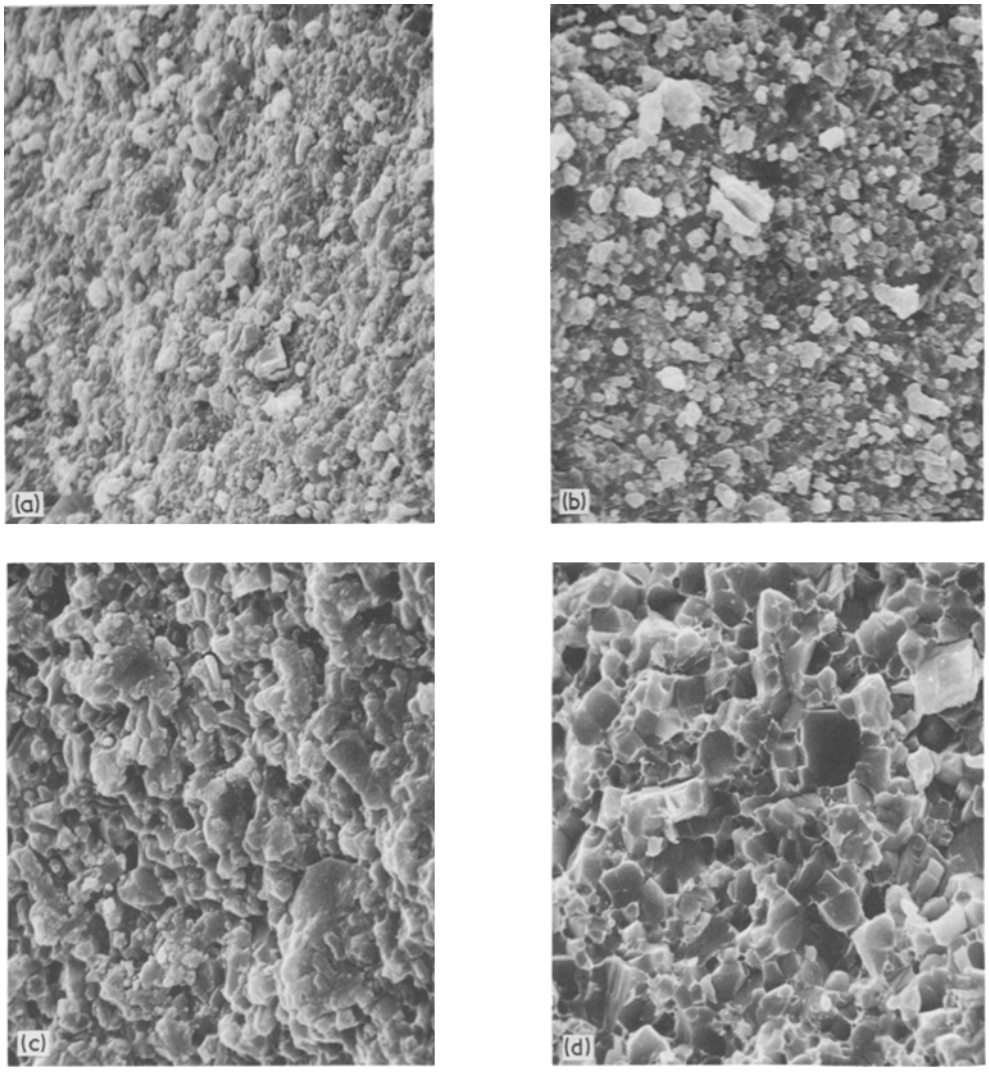

Figure 7 Typical fracture surfaces for (a) Nippon A2, within r_f (× 1300); (b) Nippon A2, outside r_f and fractured mechanically (× 1300); (c) Titan 80, within r_f (× 2600) and (d) Titan 80, outside r_f, fractured mechanically (× 2600).

Carboloy 370 respectively.

Scanning electron micrographs of typical fracture surfaces are shown in Fig. 7a to d. Fig. 7a and b relate to Nippon A2, the other pair to Titan 80. Fracture surfaces from *within* the shocked initiation regions (i.e. *within* r_f) are shown in Fig. 7a and c. The subsequent fracture surfaces produced mechanically by three-point bending at room temperature in the shocked samples (i.e. in the region *outside* r_f) appeared the *same* as those fracture surfaces *throughout* the cross-section of unshocked samples broken in three-point bending at room temperature. Typical examples are shown in Fig. 7b and d. The fracture surfaces produced by quenching through ΔT_c are more "powdery" in appearance than the room temperature surfaces.

Table V shows that the room temperature fracture toughnesses of unshocked and shocked samples are essentially the same (within our experimental error). This suggests that the reduction in room temperature retained strength after shock is caused principally by enlarged r_f. Plots of a "corrected σ_a" versus $1/\sqrt{r_f}$ should be straight lines through the origin of slope K_{IC}†.

† $K_{IC} = \sigma_a\sqrt{r_f}Y$, where Y is different for elliptical and straight starter crack geometries. Thus, Fig. 8 plots $(\sigma_a Y)$ versus $1/\sqrt{r_f}$, where $(\sigma_a Y)$ is the "corrected σ_a".

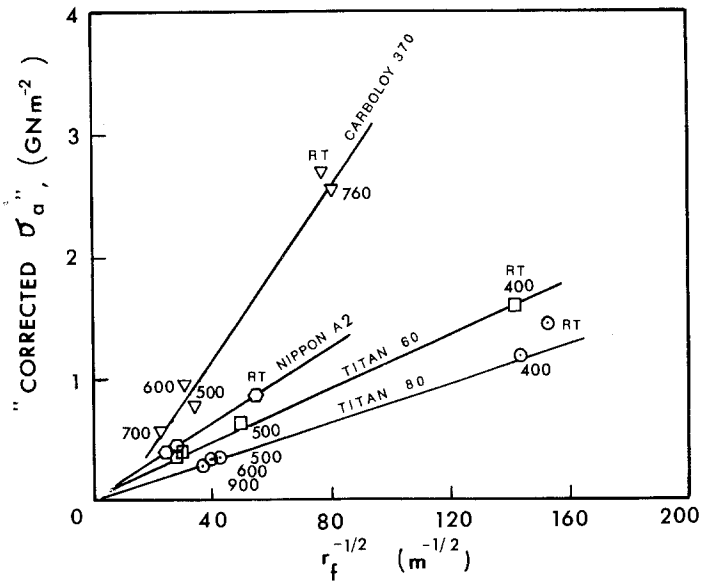

Figure 8 Plots of "corrected σ_a" versus $(r_f)^{-1/2}$ for the tool ceramics.

Fig. 8 shows the experimental results. Those materials following the Hasselman model (particularly Titan 80) "should" have a set of identical points for one flaw size at σ_f (if they have not been shocked through ΔT_c) and another set of identical points for one r_f after shocking through ΔT_c. Shocks much more severe than ΔT_c should give extra points with small $1/\sqrt{r_f}$.

It is worth mentioning that there is evidence that water retained in the samples after shocking can significantly reduce K_{IC}, sometimes by a factor of two in the case of Carboloy 370 (Table V). Some of the scatter in the room temperature K_{IC} (e.g. Carboloy 370) may be caused by such an effect, and it may be present in Fig. 8.

3.4. Correlation of strength loss and damage resistance parameter

Recently, Ainsworth and Herron have shown [2] that a modified damage resistance parameter $(ER/\sigma_f^2 V)$, calculated from room temperature property values, can be used to evaluate the loss in strength of selected refractories subjected to thermal cycling in the "brittle" temperature range (i.e. $> \Delta T_c$). Note that V is the volume of the material under stress; incorporation of V in the parameter reveals a size effect on thermal-shock-induced damage. Similar plots have been attempted for the ceramics studied here. Percentage strength losses after various thermal shocks are shown in Table VI, for all materials tested (i.e. those for which Hasselman's model is obeyed and also those not obeying the model). In general, there is no correlation when strength loss is plotted against the damage resistance parameter $(K_{IC}/\sigma_f)^2$ using room temperature values. This perhaps is not unexpected since the critical temperature differences required for crack initiation in the different ceramics vary considerably, whereas the refractories studied by Ainsworth and Herron

TABLE VI Correlation of strength loss and damage resistance parameter

Material	$(K_{IC}/\sigma_f)^2$ (mm) (R.T. values)	% strength loss				
		800° C	900° C	1000° C	1100° C	1200° C
Titan 80	0.041	89.3	89	89	90	90
Titan 60	0.097	75.4	88	88	89	90
Nippon A2	0.378	97.5	98	98	98	98
Carboloy 370	0.381	39.5	70	96	97	97
M19	1.628	14.3	24.4	40.7	58.4	73.50
C140	0.865	17.9	27.6	45.9	64.3	80.8
C132	0.736	52.2	56.3	70	78.0	98.00

Note: 1. K_{IC} and σ_f are based on R.T. measurements.
2. % strength loss $= (\sigma_f - \sigma_a)/\sigma_f \times 100\%$ where σ_f = break strength at R.T. and σ_a = strength retained after thermal shock for ten temperature cycles.

have similar ΔT_c along with instantaneous strength loss.

Despite this, some useful information can still be derived from Table VI. It may be seen that for Titan 60, Titan 80, and Nippon A2 (for all of which Hasselman's model applies) the strength loss is insensitive to the shock severity above their respective ΔT_c, whereas the strength loss of the other ceramics is highly dependent on the shock temperature, i.e. the greater the shock the more the strength loss. There are many possible reasons for this observation, amongst which the most likely is that at elevated temperatures, the magnitude of the shock damage resistance parameter is gradually diminished because of temperature variations in σ_f and $K_{IC} = \sqrt{[ER/(1-\nu^2)]}$. Then, instead of *one* $(K_{IC}/\sigma_f)^2$ value for a given material (based on room temperature values), different $(K_{IC}/\sigma_f)^2$ are appropriate to different temperatures. When the percentage strength loss resulting from shocking at a given temperature is plotted against the relevant $(K_{IC}/\sigma_f)^2$, distinct correlations are possible. To illustrate this point, the data for M19 and C140 are plotted in Fig. 9, where we see good correlation between $(1-\sigma_a/\sigma_f)$ and the $(K_{IC}/\sigma_f)^2$ varying with temperature. For both M19 and C140, K_{IC} was not measured directly, because it was impossible to make starter cracks with hardness indenters (the specimens split), and also because we could not reliably identify after breaking the very small flaws from which the final fractures occurred. Thus, E and R were separately measured as described in Section 3.3. In the case of M19, where cracking was relatively stable, confidence can be placed in the toughness values (which decreased with temperature) whereas, with C140, unstable cracking probably causes upperbound estimates for R (which were more or less independent of temperature). In addition, there is confusion as to whether E varies with temperature for C140; our results indicate that E remains constant at 74.5 GN m^{-2} between room temperature and 500° C, and then decreases linearly to 21 GN m^{-2} at 1000° C, whereas work elsewhere on the same material did not find the reduction in E. As shown in Fig. 5b the unshocked σ_f for C140 does not vary with temperature. Variations in $(K_{IC}/\sigma_f)^2$ in Fig. 9 for C140, therefore, come from variations in E and, given that the R values is an upperbound, the relationship between the parameters is satisfactory. We may note that even if E is really independent of temperature, (giving only one value for $(K_{IC}/\sigma_f)^2$) the percentage strength losses in C140 after shock, could still be explained in terms of progressively enlarged r_f after shocking. Materials which follow the Hasselman model also have a single $(K_{IC}/\sigma_f)^2$ value, for region C in Fig. 1. They also have only one $(1-\sigma_a/\sigma_f)$ value for shocking through ΔT_c because no sub-critical growth occurs for less severe shocks. On the other hand C140, even though it may have only a single $(K_{IC}/\sigma_f)^2$ value, has a varying $(1-\sigma_a/\sigma_f)$ because of sub-critical crack growth.

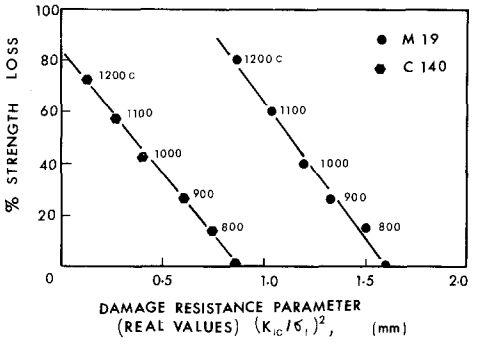

Figure 9 Correlation between thermal shock strength loss and $(K_{IC}/\sigma_f)^2$ at current high temperatures.

3.5. Effect of number of repeated shocks

In general terms, repeated shock cumulatively damage a solid by encouraging increments of "sub-critical" crack growth at every quench. Thus, σ_a decrease as the number of shocks increase, particularly for materials which do not obey the Hasselman model. That slow crack growth is the cause of smaller σ_a may be confirmed by the fact

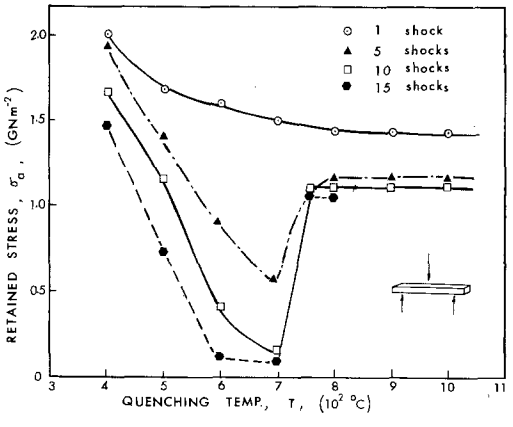

Figure 10 Variation of after shock retained strength (σ_a) with quenching temperature (T) for the lower density Carboloy 370 subjected to repeated shocks.

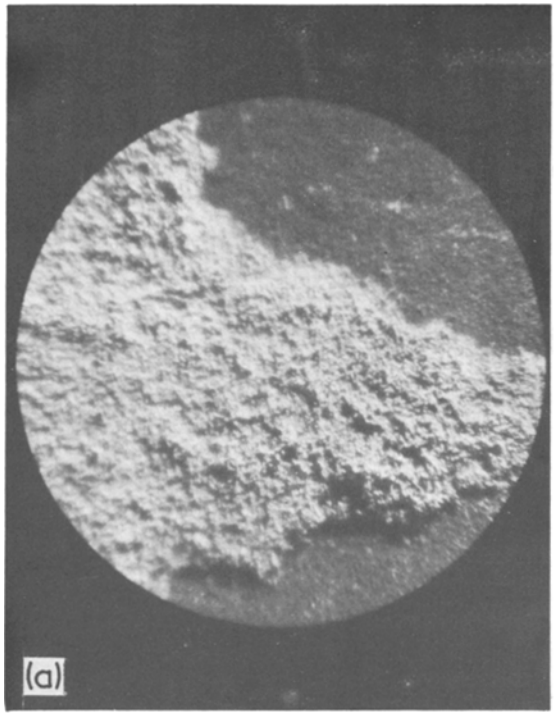

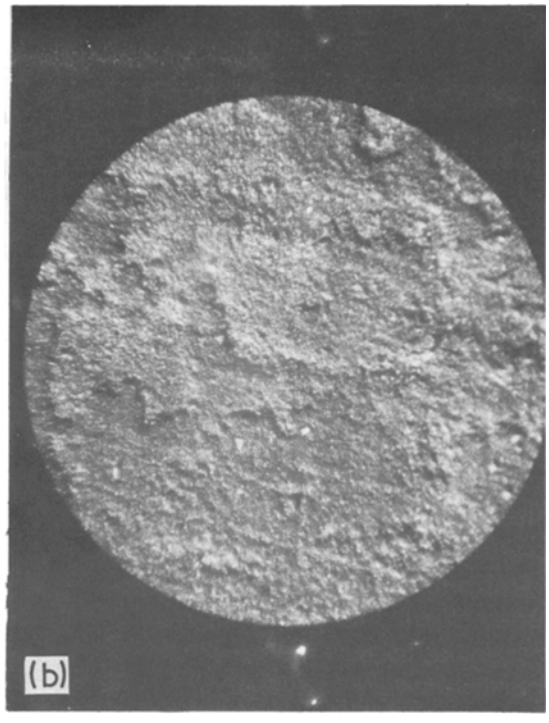

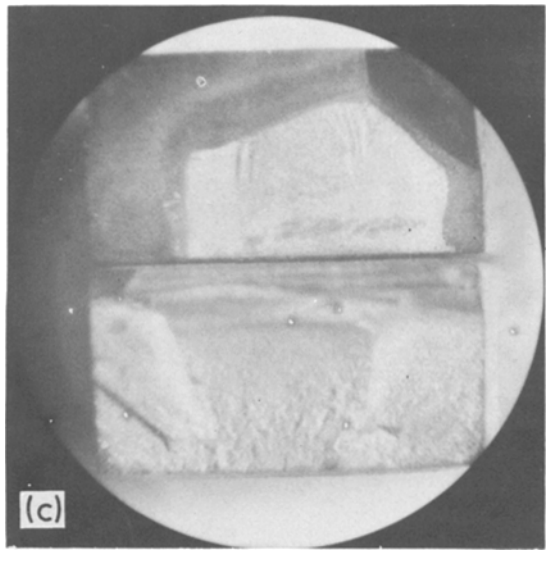

Figure 11 Typical appearances of (a) oxidized and (b) unoxidized Carboloy 370. (c) Top: fracture cross-section of unoxidized testpiece (note thermal shock induced cracks). Bottom: fracture cross-section of oxidized testpiece. (a) and (b) × 36, (c) × 10.

that the room temperature toughness of shocked samples is essentially the same as the toughness of unshocked specimens.

The behaviour of the lower density Carboloy 370 is particularly interesting. For quenching temperature differences up to about 700° C, greater numbers of repeated shocks progressively reduce the retained strength (Fig. 10). Above some 750° C, the material oxidizes very rapidly, however, and the retained strength rises again to very high levels. Notice that the single shock data do not display this behaviour. Evidently the oxidized specimens quenched many times with separate differences of at least 750° C are better able to withstand the transient shocks than the unoxidized testpieces quenched with smaller temperature differences. Fig. 11a to c show appearances of the oxidized and unoxidized specimens. Below 700° C, σ_a is reduced because of sub-critical flaw growth (cracks can be readily seen after shocking and non-linearities were observed in the load-deflection plots of the bend specimens used to determine σ_a). The density of the propagated cracks increases with the number of repeated shocks. However, after oxidation, the toughness becomes greater, so that the damage resistance parameter (K_{IC}/σ_f) increases. Thus, it is more difficult for large cracks to appear in the system, and the "undeveloped" small flaws are reflected in restored σ_a. For example, the σ_a value ($\sim 235\,MN\,m^{-2}$) after 10 shocks from 700° C is commensurate with a flaw size of about 1.5 mm; the corresponding flaw size for $\sigma_a = 1.36\,GN\,m^{-2}$ after 10 shocks from 760° C is about 0.15 mm.

On the other hand, experiments have shown

that for materials which obey Hasselman's model such as Titan 80, repeated shocks (e.g. 1 shock and 10 shocks) have negligible effects on the room temperature retained strength (σ_a). Such results should be expected and follow from Fig. 1.

3.6. Effect of strain rate on results

The strength data (for both unshocked and shocked samples) presented thus far were all obtained at a testing machine crosshead velocity of $8\,\mu m\,sec^{-1}$. Additional data for room temperature unshocked strength (σ_f) and retained after-shock strength (σ_a) were obtained as cross-head velocities

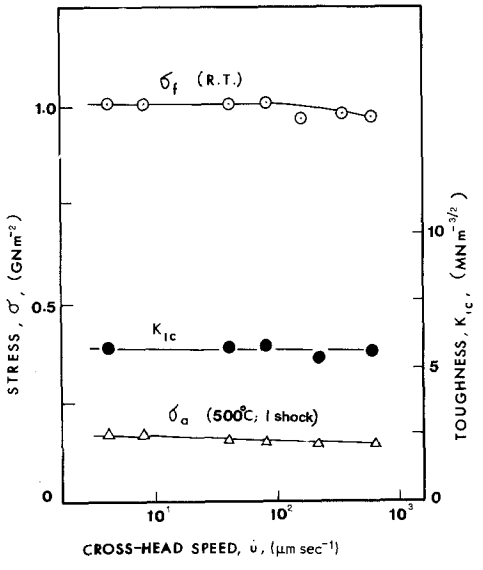

Figure 12 Variation of K_{IC}, σ_f and σ_a [1 shock at 500° C] with cross-head speed ($\dot{u}$) for Titan 80.

up to $667\,\mu m\,sec^{-1}$, as illustrated in Fig. 12 for Titan 80. Also plotted on Fig. 12 are K_{IC} data over the same range of crosshead velocities, determined from the σ_f loads and "after-the-fact" fractographic identification of the size of the "kernal" flaw from which final fracture took place; use of an appropriate fracture mechanics formula with the fracture load and flaw shape and size gives K_{IC} [21]. Both σ_f and σ_a remain comparatively constant for the complete range of cross-head speeds investigated; K_{IC} does the same.

Fig. 13 shows the rate effects on σ_a for Carboloy 370, where now the number of shocks and the temperature from which shocking took place are important. The 600° C data are lower than the 500° C, but the 1000° C results return to higher values similar to the 500° C data because of

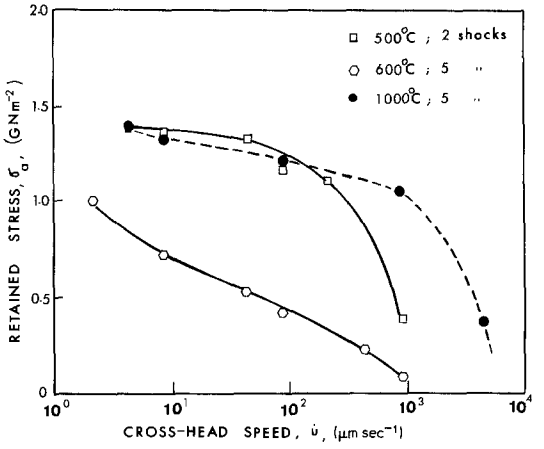

Figure 13 Effects of $\dot{u}$ on σ_a for the lower density Carboloy 370 at 3 levels of shock severities.

oxidation effects discussed previously. We do not have independent $K_{IC}(\dot{u})$ data for Carboloy 370, apart from two determinations of the room temperature K_{IC} in an unshocked sample at $8.33\,\mu m\,sec^{-1}$ cross-head speed. We may, however, take the σ_a values, investigate the fracture surfaces for the flaw from which final fracture took place, and infer K_{IC} that way. Such results are shown in Fig. 14, where it is seen that good agreement is obtained with the single unshocked K_{IC} value at the corresponding cross-head speed. Since, presumably, the flaw sizes produced after a given number of shocks from a given quenching temperature should be the same for all samples, reductions in σ_a with rate come from reductions in room temperature K_{IC} with rate such as given in Fig. 14.

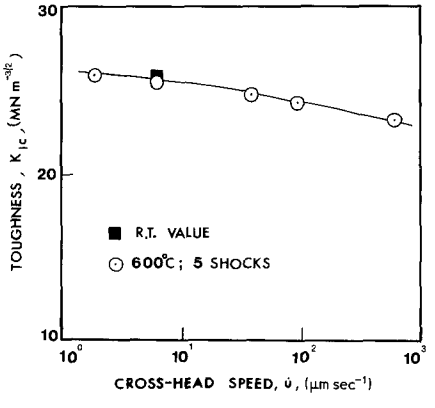

Figure 14 Effects of $\dot{u}$ on K_{IC} for Carboloy 370 subjected to 5 shocks at 600° C.

4. Conclusions

Those ceramic materials that do not follow the Hasselman model for thermal shock display a gradual reduction in retained after-shock room

temperature strength, as the severity of the quench is increased. In addition, these materials suffer cumulative damage when subjected to repeated numbers of shocks. This again contrasts with the Hasselman model which suggests that a single shock, of at least the critical quench temperature difference, fully describes the after shock retained strength behaviour. The reason for the departure from Hasselman's model seems to be bound up in reductions in fracture toughness of the ceramics with increasing temperature. Such lower toughnesses allow pre-existing flaws to initiate and grow "sub-critically" during quenches which are much less severe than the Hasselman critical temperature difference predicted from room temperature toughness and strength values. The growth of these flaws is aided by thermal fatigue which accompanies repeated shocking. That the gradual reduction in retained strength is caused principally by increasing flaw sizes is confirmed by the fact that the room temperature fracture toughness of both unshocked and shocked samples is essentially the same.

Oxidation of the Carboloy 370 cutting tool ceramic restored much of its retained strength. This suggests that the dynamic toughness of the oxidized material is greater than the unoxidized material, which, together with the ability of the oxidized layers to relax and expand freely, suggests that the chances of initiating large flaws are less when quenching from temperatures above the oxidation temperature than from below that range.

Rate of testing affects the room temperature results. In general terms, the retained after-shock strength decreases as the crosshead velocity increases because the room temperature fracture toughness decreases with increased rate.

Acknowledgements

We are most grateful to General Motors Corporation for the grant under which this study was performed. Dr F. Schierloh and his co-workers at the GM Technical Center gave us much guidance, and supplied us with the test material, some of which was specially prepared by the manufacturers concerned; (the results given here are not all necessarily therefore typical of commercial products.) We also would like to thank Mr W. H. Durrant for his help with the experiments and scanning electron microscope investigations.

References

1. J. NAKAYAMA and M. ISHIZUKA, *Amer. Ceram. Soc. Bull.* **45** (1966) 666.
2. J. H. AINSWORTH and R. H. HERON, *ibid* **53** (1974) 533.
3. D. P. H. HASSELMAN, *J. Amer. Ceram. Soc.* **52** (1969) 600.
4. *Idem, ibid* **53** (1970) 490.
5. T. K. GUPTA, *ibid.* **55** (1972) 249.
6. C. M. CHENG, *J. Amer. Rocket Soc.* **21** (1951) 147.
7. S. S. MANSON, N.A.C.A. Technical Note 2933, July 1953.
8. G. R. IRWIN, Proceedings 7th Sagamore Ordnance, Material Research Conference (1960).
9. C. GURNEY, Y. W. MAI and R. C. OWEN, *Proc. Roy. Soc. London* **A340** (1974) 213.
10. A. G. ATKINS, *Int. J. Prod. Res.* **12** (1974) 263.
11. Y. W. MAI and A. G. ATKINS, *Amer. Ceram. Soc. Bull.* **54** (1975) 593.
12. R. W. DAVIDGE and G. TAPPIN, *J. Mater. Sci.* **3** (1968) 165.
13. T. K. GUPTA, *J. Amer. Ceram. Soc.* **55** (1972) 429.
14. J. A. COPPOLA, D. A. KROHN and D. P. H. HASSELMAN, *ibid* **55** (1972) 481.
15. B. E. BERTSCH, D. R. LARSON and D. P. H. HASSELMAN, *ibid* **57** (1974) 135.
16. C. GURNEY and Y. W. MAI, *Eng. Fract. Mech.* **4**, (1972) 853.
17. Y. W. MAI and A. G. ATKINS, General Motors Technical Rept., September (1974).
18. C. GURNEY and J. HUNT, *Proc. Roy. Soc. London* **A299** (1967) 508.
19. C. GURNEY and K. M. NGAN, *ibid* A325 (1971) 207.
20. J. E. SRAWLEY and B. GROSS, ASTM, Special Technical Publications No. 410 (1966).
21. N. INGELSTROM and N. NORDBERG, *Eng. Fract. Mech.* **6** (1974) 597.
22. P. KENNY, *Powder Met.* **14** (1971) 22.
23. F. F. LANGE, Scientific Paper 73-9D4-FORAM-P1, January 2 (1973).
24. H. G. TATTERSALL and G. TAPPIN, *J. Mater. Sci* **1** (1966) 296.
25. JUNN NAKAYAMA, *J. Amer. Ceram. Soc.* **48** (1970) 583.
26. J. A. COPPOLA, R. C. BRADT, D. W. RICHERSON and R. A. ALLIEGRO, *Amer. Ceram. Soc. Bull.* **51** (1972) 847.
27. L. A. SIMPSON, *J. Amer. Ceram. Soc.* **56** (1973) 610.
28. A. T. JONES, *Engr. Fract. Mech.* **6** (1974) 435.

Received 21 March and accepted 21 April 1975.